



## Simulated bifurcation assisted by thermal fluctuation

Taro Kanao <sup>1</sup>✉ & Hayato Goto <sup>1</sup>

Various kinds of Ising machines based on unconventional computing have recently been developed for practically important combinatorial optimization. Among them, the machines implementing a heuristic algorithm called simulated bifurcation have achieved high performance, where Hamiltonian dynamics are simulated by massively parallel processing. To further improve the performance of simulated bifurcation, here we introduce thermal fluctuation to its dynamics relying on the Nosé–Hoover method, which has been used to simulate Hamiltonian dynamics at finite temperatures. We find that a heating process in the Nosé–Hoover method can assist simulated bifurcation to escape from local minima of the Ising problem, and hence lead to improved performance. We thus propose heated simulated bifurcation and demonstrate its performance improvement by numerically solving instances of the Ising problem with up to 2000 spin variables and all-to-all connectivity. Proposed heated simulated bifurcation is expected to be accelerated by parallel processing.

<sup>1</sup>Frontier Research Laboratory, Corporate Research & Development Center, Toshiba Corporation, 1, Komukai-Toshiba-cho, Saiwai-ku, Kawasaki 212-8582, Japan. ✉email: [taro.kanao@toshiba.co.jp](mailto:taro.kanao@toshiba.co.jp)

Unconventional computing with special-purpose hardware devices for solving combinatorial optimization problems has attracted growing interest due to practical importance. Many combinatorial optimization problems can be mapped onto finding ground states of Ising spin models<sup>1,2</sup>, which is referred to as the Ising problem. Special-purpose hardware devices for the Ising problem are called Ising machines. Ising machines utilizing natural phenomena have been developed, such as quantum annealers<sup>3–8</sup> with superconducting circuits<sup>9</sup>, coherent Ising machines with pulse lasers<sup>10–14</sup>, oscillator-based Ising machines<sup>15–19</sup>, and other Ising machines with various systems, such as stochastic nanomagnets<sup>20</sup>, gain-dissipative systems<sup>21</sup>, spatial light modulators<sup>22</sup>, memristor Hopfield neural networks<sup>23</sup>, and spin torque nano-oscillators<sup>24,25</sup>.

Ising machines have also been implemented with special-purpose digital processors<sup>26–32</sup> using simulated annealing (SA)<sup>33</sup> and other algorithms. Among such algorithms, simulated bifurcation (SB) is a recently proposed heuristic algorithm<sup>34</sup>. SB originates from numerical simulations of Hamiltonian dynamics with bifurcation that is a classical counterpart of quantum adiabatic bifurcation in nonlinear oscillators<sup>35,36</sup>, which itself has been studied actively<sup>37–45</sup>. Simulation-based approaches such as SB allow one to deal with dense spin–spin interactions with high precision, which might be challenging for physical implementations. Also, the classical dynamics can be simulated efficiently, unlike quantum dynamics. SB can be accelerated by parallel processing with, e.g., field-programmable gate arrays (FPGAs)<sup>34,46–48</sup>, because of its capability of simultaneous updating of variables. Recently proposed variants of SB have achieved faster and more accurate optimization<sup>49</sup> than original SB.

To further improve the performance of SB, here we introduce thermal fluctuation to SB. SA can yield high-accuracy solutions by modeling thermal fluctuation<sup>33</sup>, while quantum annealing utilizes quantum fluctuation<sup>3</sup>. These fluctuations can assist escape from local minima of the Ising problem and lead to higher solution accuracy. Our method is based on the Nosé–Hoover method<sup>50,51</sup>, which enables simulations of Hamiltonian dynamics at finite temperatures<sup>52</sup>. Unlike SA, the Nosé–Hoover method does not use random numbers, namely, is deterministic, and thus the simplicity of SB is preserved. We find that a simplified dynamics with only a heating process can improve the performance of SB, where an ancillary dynamical variable in the Nosé–Hoover method is replaced by a constant. We numerically demonstrate this improvement by solving instances of the Ising problem with up to 2000 spin variables and all-to-all connectivity, which corresponds to the Sherrington–Kirkpatrick (SK) model introduced in studies of spin glasses<sup>53–55</sup>. The SK model has been widely used to measure the performance of Ising machines<sup>12,14,28–30,32,34,49,56</sup>. Proposed heated SB is also suitable for massively parallel implementations with, e.g., FPGAs.

## Results and discussion

**SB with thermal fluctuation.** First, we briefly explain the Ising problem and SB. The Ising problem is to find  $N$  Ising spins  $s_i = \pm 1$  minimizing a dimensionless Ising energy,

$$E_{\text{Ising}} = -\frac{1}{2} \sum_{i=1}^N \sum_{j=1}^N J_{ij} s_i s_j, \quad (1)$$

where  $J_{ij}$  represents the interactions between  $s_i$  and  $s_j$  ( $J_{ij} = J_{ji}$  and  $J_{ii} = 0$ ). The SB has two latest variants, ballistic SB (bSB) and discrete SB (dSB)<sup>49</sup>. Both bSB and dSB are based on the following Hamiltonian equations of motion,

$$\dot{x}_i = a_0 y_i, \quad (2)$$

$$\dot{y}_i = -[a_0 - a(t)]x_i + c_0 f_i, \quad (3)$$

where  $x_i$  and  $y_i$  are respectively the positions and momenta corresponding to  $s_i$ , the dots denote time derivatives,  $a(t)$  is a control parameter, and  $a_0$  and  $c_0$  are constants. The force due to the interactions,  $f_i$ , are given by

$$f_i = \sum_{j=1}^N J_{ij} x_j, \quad \text{for bSB}, \quad (4)$$

$$f_i = \sum_{j=1}^N J_{ij} \text{sgn}(x_j), \quad \text{for dSB}, \quad (5)$$

where  $\text{sgn}(x_j)$  is the sign of  $x_j$ . Time evolutions of  $x_i$  are calculated by solving Eqs. (2) and (3) with the symplectic Euler method<sup>52</sup>, where the positions  $x_i$  are confined within  $|x_i| \leq 1$  by perfectly inelastic walls at  $x_i = \pm 1$ , that is, if  $|x_i| > 1$  after each time step,  $x_i$  and  $y_i$  are set to  $x_i = \text{sgn}(x_i)$  and  $y_i = 0$ . With increasing  $a(t)$  from zero to  $a_0$ , bifurcations to  $x_i = \pm 1$  occur, and the signs  $s_i = \text{sgn}(x_i)$  yield a solution to the Ising problem. A solution at the final time is at least a local minimum of the Ising problem<sup>49</sup>. Ballistic behavior in bSB leads to fast convergence to a local or approximate solution, while the discretized  $f_i$  in dSB enable higher solution accuracy with a longer time.

Here we apply the Nosé–Hoover method<sup>50–52</sup> with a finite temperature  $T$  to Eqs. (2) and (3), obtaining

$$\dot{x}_i = a_0 y_i, \quad (6)$$

$$\dot{y}_i = -[a_0 - a(t)]x_i + c_0 f_i - \xi y_i, \quad (7)$$

$$\dot{\xi} = \frac{1}{M} \left( \sum_{i=1}^N y_i^2 - NT \right), \quad (8)$$

where  $\xi$  is an ancillary variable playing a role of thermal fluctuation, and  $M$  is a parameter (mass). The variable  $\xi$  controls an instantaneous temperature defined by

$$T_{\text{inst}} = \frac{1}{N} \sum_{i=1}^N y_i^2, \quad (9)$$

to be a given  $T$  as follows. When  $T_{\text{inst}}$  is smaller than  $T$ ,  $\dot{\xi}$  is negative according to Eq. (8), which makes  $\xi$  negative. Then  $|y_i|$  increase owing to the last term in Eq. (7), and thus  $T_{\text{inst}}$  increases and approaches  $T$ , which can be regarded as heating. To the contrary, when  $T_{\text{inst}} > T$ , cooling occurs.

We found that SB gives better solutions when  $\xi$  is kept negative by negative initial  $\xi$  and large  $M$  (leading to  $\dot{\xi} \simeq 0$ ). This observation suggests that the heating can improve SB but the cooling is unnecessary. This may be because increased  $|y_i|$  by the heating can lead to escape from local minima of the Ising problem. Furthermore, small  $|\dot{\xi}|$  due to large  $M$  above implies that constant  $\xi$  can play a similar role, and then we found that  $\xi$  replaced by a negative constant  $-\gamma$  ( $\gamma > 0$ ) can rather yield higher performance. The constant  $\gamma$  is regarded as a rate of the heating.

Thus, in this paper, we propose SB with a heating term, which we call heated bSB (HbSB) and dSB (HdSB), as follows,

$$\dot{x}_i = a_0 y_i, \quad (10)$$

$$\dot{y}_i = -[a_0 - a(t)]x_i + c_0 f_i + \gamma y_i. \quad (11)$$

We numerically solve Eqs. (10) and (11) by discretizing the time by  $t_{k+1} = t_k + \Delta t$  with a time interval  $\Delta t$ , and by calculating  $x_i(t_{k+1})$  and  $y_i(t_{k+1})$  from  $x_i(t_k)$  and  $y_i(t_k)$  in each time step. Here note that the symplectic Euler method is not applicable for Eqs. (10) and (11), because these equations are no longer Hamiltonian equations owing to the term  $\gamma y_i$ <sup>52</sup>. We empirically found that solution accuracy can be improved by the same update as previous bSB and dSB<sup>49</sup> followed by an update corresponding to the term  $\gamma y_i$ . This ordering results in nonzero momenta by the

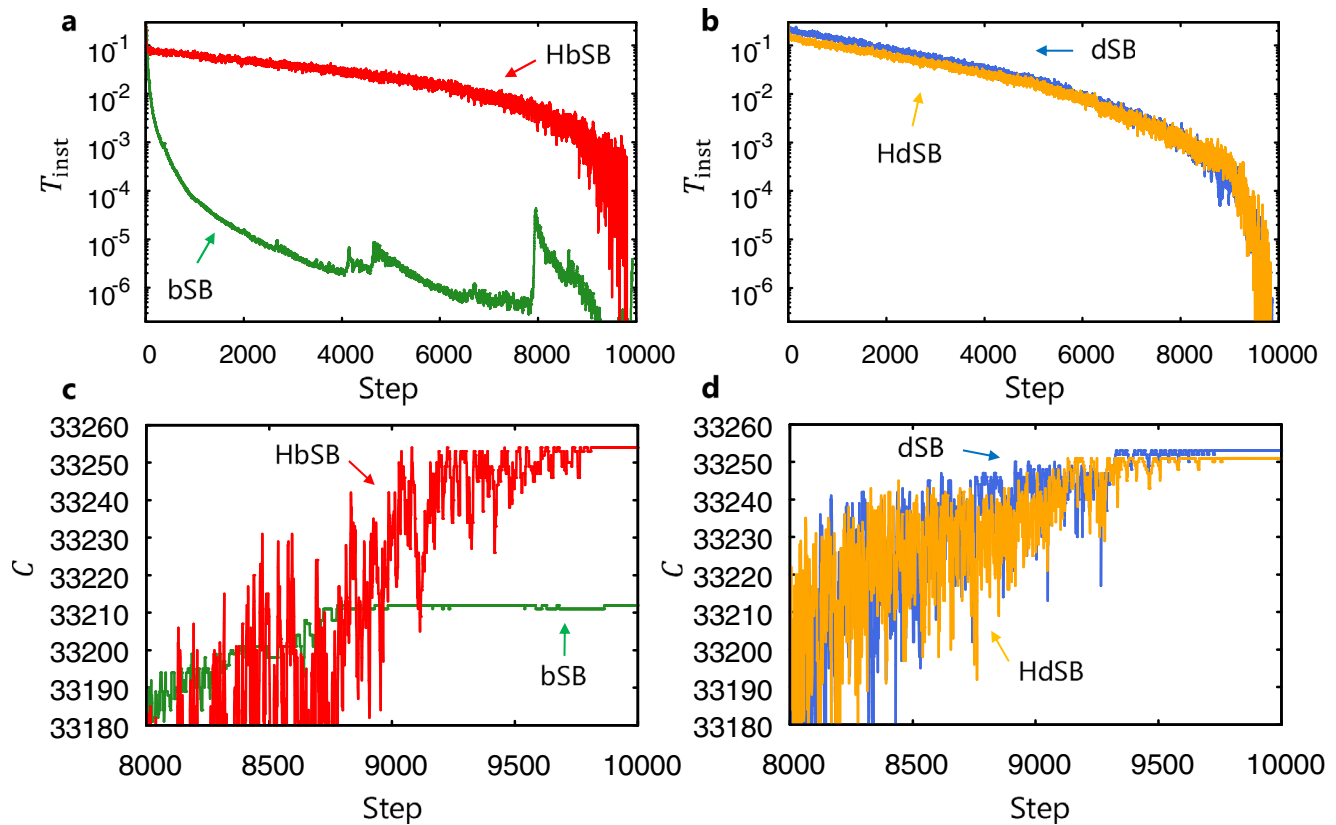


**Fig. 1 Time evolutions in simulated bifurcation (SB) for a 2000-spin Ising problem ( $K_{2000}$ ).** **a, b** Instantaneous temperatures  $T_{\text{inst}}$ . **c, d** Instantaneous cut values  $C$ . Here, bSB, dSB, HbSB, and HdSB denote ballistic SB, discrete SB, heated bSB, and heated dSB, respectively. Time is represented by time steps. Parameters are  $\Delta t = 0.7$  and  $c_1 = 0.6$  for bSB,  $\Delta t = 1.1$  and  $c_1 = 0.6$  for dSB,  $\Delta t = 1.1$ ,  $c_1 = 0.9$  and  $\gamma = 0.5$  for HbSB, and  $\Delta t = 1.1$ ,  $c_1 = 0.7$  and  $\gamma = 0.06$  for HdSB.

heating and can prevent from getting stuck at the walls. See “Methods” for a detailed algorithm.

In the following, we compare heated SB with previous SB by solving instances of the Ising problem with all-to-all connectivity, where  $J_{ij}$  are randomly chosen from  $\pm 1$  with equal probabilities (corresponding to the SK model). The control parameter  $a(t)$  is linearly increased from 0 to  $a_0$ . The constant parameters are set as  $a_0 = 1$  and

$$c_0 = \frac{c_1}{\sqrt{N}}, \quad (12)$$

where  $c_1$  is a parameter tuned around 0.5, which is based on random matrix theory<sup>34,49</sup>.  $x_i$  and  $y_i$  are initialized by uniform random numbers in the interval  $(-1, 1)$ .

**Performance for a 2000-spin Ising problem.** We first solve a benchmark instance called  $K_{2000}$ , which is a 2000-spin instance of the Ising problem with all-to-all connectivity<sup>12,30,34,49</sup>.  $K_{2000}$  is often expressed as a MAX-CUT problem. The MAX-CUT problem is given by weights  $w_{ij}$  with  $w_{ij} = w_{ji}$ , and the following cut value  $C$  is maximized,

$$C = \frac{1}{2} \sum_{i=1}^N \sum_{j=1}^N w_{ij} \frac{1 - s_i s_j}{2} \quad (13)$$

$$= -\frac{1}{2} E_{\text{Ising}} - \frac{1}{4} \sum_{i=1}^N \sum_{j=1}^N J_{ij}, \quad (14)$$

where in Eq. (14),  $C$  has been related to  $E_{\text{Ising}}$  [Eq. (1)] by  $w_{ij} = -J_{ij}$ . Thus the MAX-CUT problem can be reduced to the Ising problem.

To confirm the effect of the heating, we calculate the instantaneous temperature  $T_{\text{inst}}$  in Eq. (9) and the cut value  $C$

in Eq. (14) at every time step. Figure 1a, b shows typical examples of time evolutions of  $T_{\text{inst}}$ . Here parameters are the ones optimized in advance, which are explained later. For bSB,  $T_{\text{inst}}$  rapidly decreases owing to collisions with the perfectly inelastic walls, while  $T_{\text{inst}}$  for HbSB is kept much higher owing to the heating, as expected. For dSB,  $T_{\text{inst}}$  is also higher than bSB, because the discretized forces  $f_i$  in Eq. (5) increase energy, violating conservation of energy<sup>49</sup>. In comparison between HbSB and dSB,  $T_{\text{inst}}$  for HbSB is higher than dSB around the end of the evolution. HdSB shows similar  $T_{\text{inst}}$  to dSB, implying that the heating does not alter the dynamics of dSB.

Figure 1c, d shows last parts of typical time evolutions of  $C$ . (These final  $C$  are at around the middle of distributions in many trials, not the best ones, which we will see in Fig. 2). For bSB,  $C$  is almost constant for the last 1000 time steps, while  $C$  for HbSB continues to fluctuate until nearly the end of the evolution owing to the heating. The fluctuation for HbSB looks similar to the fluctuations for dSB and HdSB.

Next, we solve  $K_{2000}$  in  $10^4$  trials with random initial  $x_i$  and  $y_i$ . In one trial,  $C$  is evaluated every 100 time steps, and the best value is output. Figure 2 shows examples of cumulative distributions of  $C$ , where the number of trials giving cut values lower than  $C$  are normalized by the total number of trials,  $10^4$ . For bSB, the majority of trials results in one of a few values of  $C$  between 33200 and 33300. On the other hand, dSB, HbSB, and HdSB yield broader distributions, owing to fluctuations (higher instantaneous temperatures) in their dynamics. It is notable that the heating changes the distribution of bSB to the one similar to the distribution of dSB (and HdSB), and that the heating much improves bSB. The insets in Fig. 2 show magnifications around the best known cut value,  $C_{\text{best}} = 33337$ <sup>49</sup>. The distributions for dSB and HdSB are almost overlapping, indicating the similar

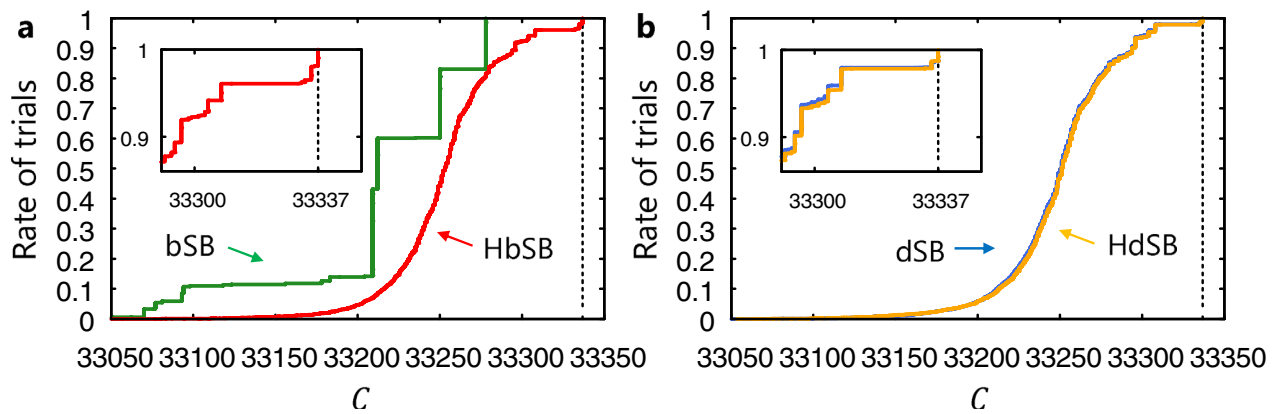


**Fig. 2** Cumulative distributions of cut values  $C$  for  $K_{2000}$ . **a** For bSB and HbSB. **b** For dSB and HdSB. (SB means simulated bifurcation, and b, d, and H denote ballistic, discrete, and heated, respectively.) The dashed vertical line indicates the best known cut value 33337. Insets show magnifications around the best known cut value. Here the number of time steps is  $N_s = 10000$ , and parameters  $\Delta t$ ,  $c_1$ , and  $\gamma$  are the same as in Fig. 1.

performance of dSB and HdSB. The insets also show that HbSB leads to more trials resulting in  $C$  close to  $C_{\text{best}}$  than dSB and HdSB, suggesting the highest performance of HbSB.

We then evaluate average and maximum  $C$  in the  $10^4$  trials and probability  $P$  for obtaining  $C_{\text{best}}$ . Here,  $P$  is estimated by dividing the number of trials obtaining  $C_{\text{best}}$  by the total number of trials. Also, using  $P$  and the number of time steps,  $N_s$ , we calculate the number of time steps required to find  $C_{\text{best}}$  with a probability of 99%, which we call step-to-solution  $S$ , given by

$$S = N_s \frac{\log 0.01}{\log(1 - P)}. \quad (15)$$

Step-to-solution is a useful measure of performance of an algorithm<sup>32</sup>. (Time-to-solution is often used to measure performance of Ising machines<sup>28,31,32,49</sup>, but it depends on not only algorithms but also implementations to hardware devices. Time-to-solution equals step-to-solution multiplied by a computation time for one time step.) Here the parameters  $\Delta t$ ,  $c_1$ , and  $\gamma$  are set such that  $S$  are minimized. For bSB, instead, average  $C$  is maximized, because we found  $P = 0$  for bSB and could not estimate  $S$ .

Figure 3a shows average and maximum  $C$  as functions of  $N_s$ . For large  $N_s$ , average  $C$  for dSB, HbSB, and HdSB are larger than that for bSB.  $C_{\text{best}}$  is reached by three SBs other than bSB. Figure 3b shows that, for large  $N_s$ ,  $P$  are the highest for HbSB, followed by HdSB, dSB, and bSB in this ordering.

Figure 3c shows  $S$  as functions of  $N_s$ . Each SB has a minimum of  $S$  at certain  $N_s$ , and in the following we compare  $S$  minimized with respect to  $N_s$ . The black cross represents a value obtained from previously reported data for dSB<sup>49</sup>. The present value of  $S$  for dSB is smaller than the previous value, because in this study the parameters  $\Delta t$  and  $c_1$  are optimized for  $K_{2000}$  while not in the previous study. In Fig. 3c, at optimal  $N_s$ ,  $S$  for HbSB is the smallest. Compared with dSB,  $S$  are reduced by 32.7% for HbSB and 19.7% for HdSB. These results demonstrate that the heating improves the performance. Although dSB performs better than bSB, bSB is much more improved by the heating than dSB, and resulting HbSB shows higher performance than HdSB.

### Performance for 100 instances of a 700-spin Ising problem.

Finally, we examine the performance for instances other than  $K_{2000}$  by solving 100 instances of the Ising problem with 700 spin variables and all-to-all connectivity<sup>32,49</sup>. For these instances, reference solutions for estimating step-to-solution were obtained by SA with sufficiently long annealing times and many iterations, which are expected to be close to optimal solutions<sup>49</sup>. Here each

instance is solved in  $10^4$  trials, and  $C$  (or  $E_{\text{Ising}}$ ) is evaluated at the last time step. We set the parameters to the values optimized in  $K_{2000}$ .

Figure 4 shows the medians of  $S$  for the 100 instances<sup>32,49</sup> as functions of  $N_s$ .  $S$  by dSB, HbSB, and HdSB are much smaller than  $S$  by bSB, because larger fluctuations in these three SBs might assist escape from local minima, as suggested in Figs. 1 and 2 for  $K_{2000}$ . Besides, HbSB results in the smallest  $S$  among four SBs. In comparison with dSB, HbSB reduces  $S$  by 9.55%. This result demonstrates that HbSB can improve the performance for not only  $K_{2000}$  but also the other instances. The reason for the highest performance of HbSB is left for future work.

### Conclusions

We have demonstrated that SB can be improved by introducing fluctuation with a heating term, which has been obtained by replacing an ancillary dynamical variable in the Nosé-Hoover method by a constant rate of heating. We have compared previous and heated SBs by solving all-to-all connected 2000-spin and 700-spin instances of the Ising problem (the SK model), and have found that HbSB gives better step-to-solution than bSB, dSB, and HdSB. This result indicates that the heating is effective, especially for bSB.

Since the proposed heated SB shares the simple dynamics with previous SB, we expect that heated SB will be accelerated by massively parallel processing implemented by, e.g., FPGAs. This study also implies that further improvements of SB will be possible by simple physics-inspired modifications like the heating term introduced here. For example, fluctuations in Hamiltonian dynamics can also be modeled by stochastic methods<sup>57</sup>.

### Methods

**Heated simulated bifurcation.** First, the symplectic Euler method<sup>52</sup> is formally applied to the terms other than  $\gamma y_i$  in Eqs. (10) and (11),

$$\tilde{y}_i = y_i(t_k) + \{-[a_0 - a(t_k)]x_i(t_k) + c_0 f_i\} \Delta t, \quad (16)$$

$$\tilde{x}_i = x_i(t_k) + a_0 \tilde{y}_i \Delta t, \quad (17)$$

where  $f_i$  are calculated from  $x_i(t_k)$  with Eqs. (4) and (5), and the variables with the tildes denote temporary variables used within a time step. Then, the perfectly inelastic walls work as

$$x_i(t_{k+1}) = g(\tilde{x}_i), \quad (18)$$

$$\tilde{y}_i = h(\tilde{x}_i, \tilde{y}_i), \quad (19)$$

where the functions  $g(x)$  and  $h(x, y)$  are given by

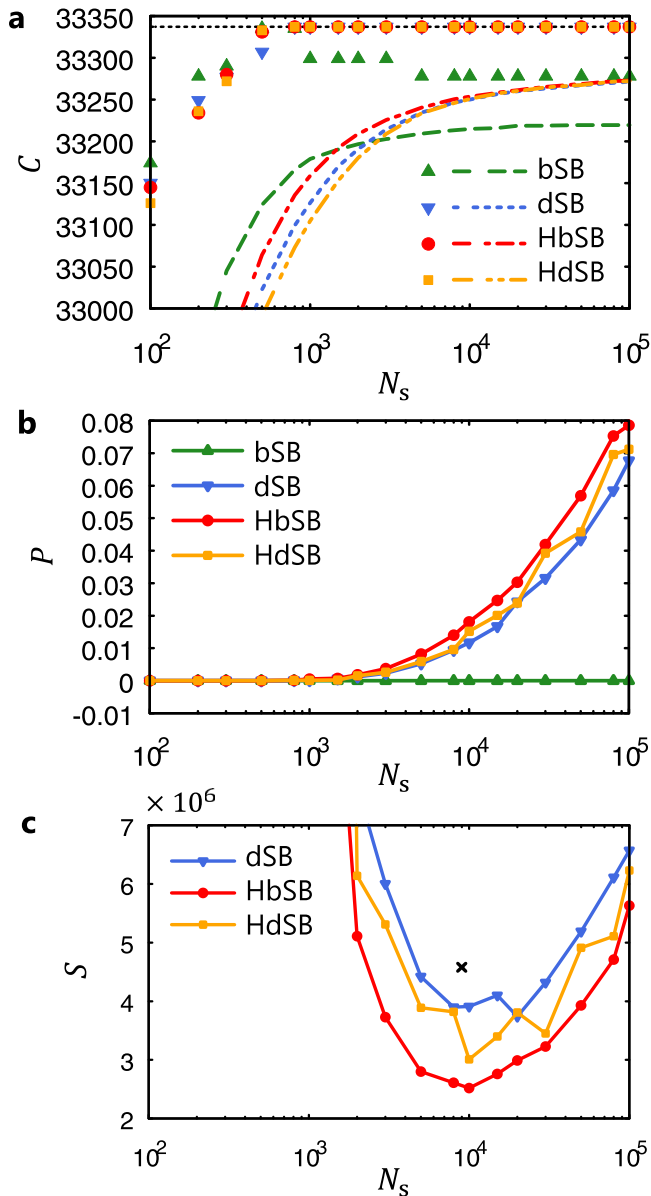


**Fig. 3 Comparison of performance for K<sub>2000</sub>.** **a** Average (lines) and maximum (symbols) cut values  $C$  as functions of the number of time steps,  $N_s$ . The horizontal dashed line indicates the best known cut value  $C_{\text{best}} = 33337$ . The maximum  $C$  for dSB, HbSB, and HdSB coincide with  $C_{\text{best}}$  for  $N_s \geq 800$ . **b** Probabilities for obtaining  $C_{\text{best}}$ ,  $P$ . **c** Step-to-solution  $S$ . The black cross is step-to-solution obtained from previously reported data for dSB<sup>49</sup>. Parameters  $\Delta t$ ,  $c_1$ , and  $\gamma$  here are the same as in Fig. 1. SB means simulated bifurcation, and b, d, and H denote ballistic, discrete, and heated, respectively.

$$g(x) = \begin{cases} x, & |x| \leq 1, \\ 1, & x > 1, \\ -1, & x < -1, \end{cases} \quad (20)$$

$$h(x, y) = \begin{cases} y, & |x| \leq 1, \\ 0, & |x| > 1. \end{cases} \quad (21)$$

Finally, we include the heating term, referring to the usual Euler method, as

$$y_i(t_{k+1}) = \tilde{y}_i + \gamma y_i(t_k) \Delta t. \quad (22)$$

Equations (16)–(19) and (22) are numerically solved, where the variables are represented as single precision floating-point real numbers.

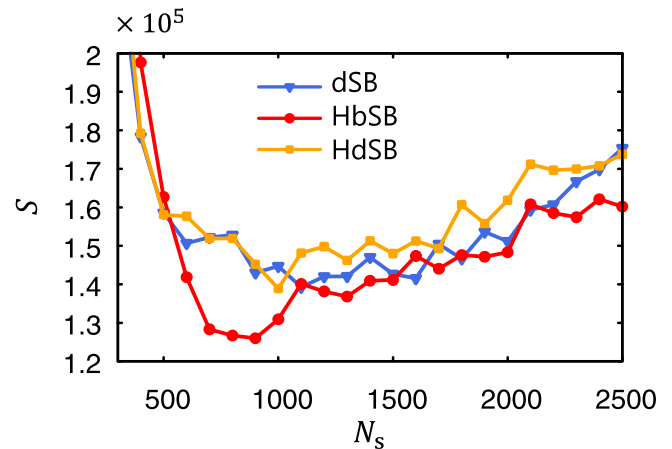


**Fig. 4 Comparison of performance for 100 instances of a 700-spin Ising problem.** The medians of step-to-solution  $S$  for the 100 instances are shown as functions of the number of time steps,  $N_s$ . Parameters  $\Delta t$ ,  $c_1$ , and  $\gamma$  are the same as in Fig. 1. SB means simulated bifurcation, and b, d, and H denote ballistic, discrete, and heated, respectively.

#### Data availability

The data that support the findings of this study are available from the corresponding author upon reasonable request.

#### Code availability

The code used in this work is available from the corresponding author upon reasonable request.

Published online: 14 June 2022

#### References

- Barahona, F. On the computational complexity of Ising spin glass models. *J. Phys. A: Math. Gen.* **15**, 3241–3253 (1982).
- Lucas, A. Ising formulations of many NP problems. *Front. Phys.* **2**, 5 (2014).
- Kadowaki, T. & Nishimori, H. Quantum annealing in the transverse Ising model. *Phys. Rev. E* **58**, 5355–5363 (1998).
- Farhi, E., Goldstone, J., Gutmann, S. & Sipser, M. Quantum computation by adiabatic evolution. Preprint at <https://arxiv.org/abs/quant-ph/0001106> (2000).
- Farhi, E. et al. A quantum adiabatic evolution algorithm applied to random instances of an NP-complete problem. *Science* **292**, 472–475 (2001).
- Das, A. & Chakrabarti, B. K. Colloquium: Quantum annealing and analog quantum computation. *Rev. Mod. Phys.* **80**, 1061–1081 (2008).
- Albash, T. & Lidar, D. A. Adiabatic quantum computation. *Rev. Mod. Phys.* **90**, 015002 (2018).
- Hauke, P., Katzgraber, H. G., Lechner, W., Nishimori, H. & Oliver, W. D. Perspectives of quantum annealing: methods and implementations. *Rep. Prog. Phys.* **83**, 054401 (2020).
- Johnson, M. W. et al. Quantum annealing with manufactured spins. *Nature* **473**, 194–198 (2011).
- Wang, Z., Marandi, A., Wen, K., Byer, R. L. & Yamamoto, Y. Coherent Ising machine based on degenerate optical parametric oscillators. *Phys. Rev. A* **88**, 063853 (2013).
- Marandi, A., Wang, Z., Takata, K., Byer, R. L. & Yamamoto, Y. Network of time-multiplexed optical parametric oscillators as a coherent Ising machine. *Nat. Photonics* **8**, 937–942 (2014).
- Inagaki, T. et al. A coherent Ising machine for 2000-node optimization problems. *Science* **354**, 603–606 (2016).
- Yamamoto, Y. et al. Coherent Ising machines—optical neural networks operating at the quantum limit. *npj Quantum Inf.* **3**, 49 (2017).
- Honjo, T. et al. 100,000-spin coherent Ising machine. *Sci. Adv.* **7**, eab0952 (2021).
- Wang, T. & Roychowdhury, J. Oscillator-based Ising machine. Preprint at <https://arxiv.org/abs/1709.08102> (2017).



16. Wang, T. & Roychowdhury, J. *Unconventional Computation and Natural Computation. UCNC 2019. Lecture Notes in Computer Science* Vol. 11493, 232–256 (Springer, 2019).
17. Chou, J., Bramhavar, S., Ghosh, S. & Herzog, W. Analog coupled oscillator based weighted Ising machine. *Sci. Rep.* **9**, 14786 (2019).
18. Mallick, A. et al. Using synchronized oscillators to compute the maximum independent set. *Nat. Commun.* **1**, 4689 (2020).
19. Vaidya, J., Kanthi, R. S. & Shukla, N. Creating electronic oscillator-based Ising machines without external injection locking. *Sci. Rep.* **12**, 981 (2022).
20. Sutton, B., Camsari, K. Y., Behin-Aein, B. & Datta, S. Intrinsic optimization using stochastic nanomagnets. *Sci. Rep.* **7**, 44370 (2017).
21. Kalinin, K. P. & Berloff, N. G. Global optimization of spin Hamiltonians with gain-dissipative systems. *Sci. Rep.* **8**, 17791 (2018).
22. Pierangeli, D., Marcucci, G. & Conti, C. Large-scale photonic Ising machine by spatial light modulation. *Phys. Rev. Lett.* **122**, 213902 (2019).
23. Cai, F. et al. Power-efficient combinatorial optimization using intrinsic noise in memristor Hopfield neural networks. *Nat. Electron.* **3**, 409–418 (2020).
24. Houshang, A. et al. A spin Hall Ising machine. Preprint at <https://arxiv.org/abs/2006.02236> (2020).
25. Albertsson, D. I. et al. Ultrafast Ising machines using spin torque nano-oscillators. *Appl. Phys. Lett.* **118**, 112404 (2021).
26. Yamaoka, M. et al. A 20k-spin Ising chip to solve combinatorial optimization problems with CMOS annealing. *IEEE J. Solid-State Circuits* **51**, 303–309 (2016).
27. Tsukamoto, S., Takatsu, M., Matsubara, S. & Tamura, H. An accelerator architecture for combinatorial optimization problems. *FUJITSU Sci. Tech. J.* **53**, 8–13 (2017).
28. Aramon, M. et al. Physics-inspired optimization for quadratic unconstrained problems using a digital annealer. *Front. Phys.* **7**, 48 (2019).
29. Okuyama, T., Sonobe, T., Kawarabayashi, K. & Yamaoka, M. Binary optimization by momentum annealing. *Phys. Rev. E* **100**, 012111 (2019).
30. Yamamoto, K. et al. STATICA: A 512-spin 0.25M-weight annealing processor with an all-spin-updates-at-once architecture for combinatorial optimization with complete spin–spin interactions. *IEEE J. Solid-State Circuits* **56**, 165–178 (2021).
31. Patel, S., Chen, L., Canoza, P. & Salahuddin, S. Ising model optimization problems on a FPGA accelerated restricted Boltzmann machine. Preprint at <https://arxiv.org/abs/2008.04436> (2020).
32. Leleu, T. et al. Scaling advantage of chaotic amplitude control for high-performance combinatorial optimization. *Commun. Phys.* **4**, 266 (2021).
33. Kirkpatrick, S., Gelatt, C. D. & Vecchi, M. P. Optimization by simulated annealing. *Science* **220**, 671–680 (1983).
34. Goto, H., Tatsumura, K. & Dixon, A. R. Combinatorial optimization by simulating adiabatic bifurcations in nonlinear Hamiltonian systems. *Sci. Adv.* **5**, eaav2372 (2019).
35. Goto, H. Bifurcation-based adiabatic quantum computation with a nonlinear oscillator network. *Sci. Rep.* **6**, 21686 (2016).
36. Goto, H. Quantum computation based on quantum adiabatic bifurcations of Kerr-nonlinear parametric oscillators. *J. Phys. Soc. Jpn.* **88**, 061015 (2019).
37. Nigg, S. E., Lörch, N. & Tiwari, R. P. Robust quantum optimizer with full connectivity. *Sci. Adv.* **3**, e1602273 (2017).
38. Puri, S., Andersen, C. K., Grimsom, A. L. & Blais, A. Quantum annealing with all-to-all connected nonlinear oscillators. *Nat. Commun.* **8**, 15785 (2017).
39. Zhao, P. et al. Two-photon driven Kerr resonator for quantum annealing with three-dimensional circuit QED. *Phys. Rev. Appl.* **10**, 024019 (2018).
40. Goto, H., Lin, Z. & Nakamura, Y. Boltzmann sampling from the Ising model using quantum heating of coupled nonlinear oscillators. *Sci. Rep.* **8**, 7154 (2018).
41. Kewming, M. J., Shrapnel, S. & Milburn, G. J. Quantum correlations in the Kerr Ising model. *N. J. Phys.* **22**, 053042 (2020).
42. Onodera, T., Ng, E. & McMahon, P. L. A quantum annealer with fully programmable all-to-all coupling via Floquet engineering. *npj Quantum Inf.* **6**, 48 (2020).
43. Goto, H. & Kanao, T. Quantum annealing using vacuum states as effective excited states of driven systems. *Commun. Phys.* **3**, 235 (2020).
44. Kanao, T. & Goto, H. High-accuracy Ising machine using Kerr-nonlinear parametric oscillators with local four-body interactions. *npj Quantum Inf.* **7**, 18 (2021).
45. Goto, H. & Kanao, T. Chaos in coupled Kerr-nonlinear parametric oscillators. *Phys. Rev. Res.* **3**, 043196 (2021).
46. Tatsumura, K., Dixon, A. R. & Goto, H. FPGA-based simulated bifurcation machine. In *2019 29th International Conference on Field Programmable Logic and Applications (FPL)*, 59–66 (IEEE, New York, 2019).
47. Zou, Y. & Lin, M. Massively simulating adiabatic bifurcations with FPGA to solve combinatorial optimization. In *Proceedings of the 2020 ACM/SIGDA International Symposium on Field-Programmable Gate Arrays (FPGA '20)*, 65–75 (ACM, New York, 2020).
48. Tatsumura, K., Yamasaki, M. & Goto, H. Scaling out Ising machines using a multi-chip architecture for simulated bifurcation. *Nat. Electron.* **4**, 208–217 (2021).
49. Goto, H. et al. High-performance combinatorial optimization based on classical mechanics. *Sci. Adv.* **7**, eaab7953 (2021).
50. Nosé, S. A molecular dynamics method for simulations in the canonical ensemble. *Mol. Phys.* **52**, 255–268 (1984).
51. Hoover, W. G. Canonical dynamics: Equilibrium phase-space distributions. *Phys. Rev. A* **31**, 1695–1697 (1985).
52. Leimkuhler, B. & Reich, S. *Simulating Hamiltonian Dynamics* (Cambridge University Press, 2004).
53. Sherrington, D. & Kirkpatrick, S. Solvable model of a spin-glass. *Phys. Rev. Lett.* **35**, 1792–1796 (1975).
54. Parisi, G. Infinite number of order parameters for spin-glasses. *Phys. Rev. Lett.* **43**, 1754–1756 (1979).
55. Parisi, G., Ritort, F. & Slanina, F. Critical finite-size corrections for the Sherrington–Kirkpatrick spin glass. *J. Phys. A: Math. Gen.* **26**, 247–259 (1993).
56. Oshiyama, H. & Ohzeki, M. Benchmark of quantum-inspired heuristic solvers for quadratic unconstrained binary optimization. *Sci. Rep.* **12**, 2146 (2022).
57. Andersen, H. C. Molecular dynamics simulations at constant pressure and/or temperature. *J. Chem. Phys.* **72**, 2384 (1980).

## Acknowledgements

We thank K. Tatsumura, R. Hidaka, Y. Hamakawa, M. Yamasaki, and Y. Sakai for valuable discussion.

## Author contributions

T.K. and H.G. conceived the idea, and developed the code. T.K. performed the numerical simulations presented here. T.K. and H.G. wrote the manuscript. H.G. supervised this project.

## Competing interests

T.K. and H.G. are inventors on Japanese, US, and Chinese patent applications related to this work filed by Toshiba Corporation (no. P2021-036688, filed 8 March 2021, no. 17/461452, filed 30 August 2021, and no. 202111002962.7, filed 30 August 2021, respectively). The authors declare no other competing interests.

## Additional information

**Correspondence** and requests for materials should be addressed to Taro Kanao.

**Peer review information** *Communications Physics* thanks the anonymous reviewers for their contribution to the peer review of this work.

**Reprints and permission information** is available at <http://www.nature.com/reprints>

**Publisher's note** Springer Nature remains neutral with regard to jurisdictional claims in published maps and institutional affiliations.



**Open Access** This article is licensed under a Creative Commons Attribution 4.0 International License, which permits use, sharing, adaptation, distribution and reproduction in any medium or format, as long as you give appropriate credit to the original author(s) and the source, provide a link to the Creative Commons license, and indicate if changes were made. The images or other third party material in this article are included in the article's Creative Commons license, unless indicated otherwise in a credit line to the material. If material is not included in the article's Creative Commons license and your intended use is not permitted by statutory regulation or exceeds the permitted use, you will need to obtain permission directly from the copyright holder. To view a copy of this license, visit <http://creativecommons.org/licenses/by/4.0/>.

© The Author(s) 2022